

Modification of the solid-state structure of bis(1-hydroxy-2(1*H*)-pyridinethiolato-*S*²,*O*)zinc(II): synthesis and characterisation of a molecular solid solution incorporating 3-hydroxy-4-methyl-2(3*H*)-thiazolethione†

Andrew D. Bond,* Francesca Benevelli and William Jones

University of Cambridge, Department of Chemistry, Lensfield Road, Cambridge, UK CB2 1EW. Tel: +44 1223 336352; Fax: +44 1223 336362; E-mail: adb29@cam.ac.uk

Received 25th July 2001, Accepted 25th October 2001

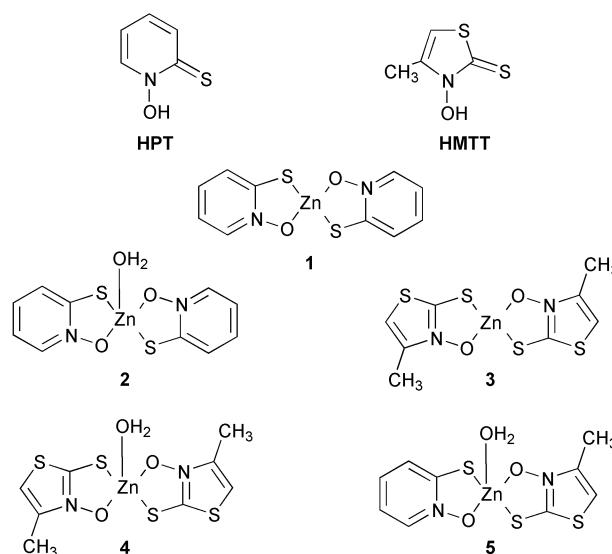
First published as an Advance Article on the web 18th December 2001

A molecular solid solution incorporating hydrated divalent zinc complexes of the fungicidal materials 1-hydroxy-2(1*H*)-pyridinethione (pyrithione, HPT) and 3-hydroxy-4-methyl-2(3*H*)-thiazolethione (methylthiazolethione, HMTT) has been synthesised over the composition range $\text{Zn}(\text{PT})_x(\text{MTT})_{2-x}(\text{H}_2\text{O})$, $1 \leq x \leq 2$. The material has been characterised by single-crystal X-ray diffraction, but extensive crystallographic disorder prohibits unambiguous identification of the molecular species present in the crystal. This ambiguity may be resolved by consideration of the identity of the material following dehydration, as probed by high-temperature powder X-ray diffraction and solid-state ^1H - ^{13}C CP/MAS NMR. These techniques suggest that the material consists of a solid solution of $\text{Zn}(\text{PT})_2(\text{H}_2\text{O})$ in an orientationally-disordered lattice of $\text{Zn}(\text{PT})(\text{MTT})(\text{H}_2\text{O})$.

Introduction

The bulk physicochemical properties of molecular materials depend not only on molecular structure, but also on the arrangement adopted by molecules in the solid state.^{1,2} Thus, different solid-state arrangements of the same molecule (polymorphs) can display markedly different properties, and control of solid-state structure is essential to exploit successfully the bulk properties of molecules. As knowledge of the relationship between solid-state structure and physicochemical properties develops for a particular class of materials, there arises the possibility of tailoring structures for applications where specific properties are desirable. Modification of solid-state structure in a controlled manner may allow for production of structural variants of existing molecules with properties enhanced for specific applications. Strategies for structure modification include isolation of polymorphs,^{3,4} production of solvates or hydrates,⁵ and formation of mixed-molecular solids (including both stoichiometric co-crystals and non-stoichiometric solid solutions).^{6–8}

Recently, we have been studying the solid-state chemistry of a number of cyclic thiohydroxamic acids.⁹ The motivation for this research arises predominantly from the biocidal properties of the materials: 1-hydroxy-2(1*H*)-pyridinethione (pyrithione, HPT),^{10,11} for example, finds extensive application as a fungicide, and the divalent zinc complex of pyrithione [$\text{Zn}(\text{PT})_2$, **1**] is the active ingredient in most antidandruff shampoos.¹² For this reason, we have been particularly interested in the zinc complex **1** and in the possibility of modifying its solid-state structure to give rise to modified bulk physicochemical properties. The strategy of solvate/hydrate formation has led previously to the synthesis and characterisation of the novel hydrate $\text{Zn}(\text{PT})_2(\text{H}_2\text{O})$ **2**.¹³



In this work, we focus on a second strategy for structure modification, namely co-crystal formation. It may be envisaged that successful co-crystallisation of two active molecular species will give rise to a composite material which possesses the activity of both components. If the two components have complementary properties (e.g. one biocidal component fills gaps in the activity spectrum of the second), co-crystallisation will lead to a combined material with a complete spectrum of desirable properties. If the materials in question were to be applied in solution, it might be expected that application of a co-crystal would ultimately be equivalent to application of a physical mixture. Co-crystallisation, however, modifies the solid-state structure of each component, such that the combined material may display bulk properties different from those of a physical mixture.

It has been suggested that the fungicidal activity of **1** may be

†Electronic supplementary information (ESI) available: lists of reflection indices and refined lattice parameters from the PXRD profiles of the single phase $\text{Zn}(\text{PT})_x(\text{MTT})_{2-x}(\text{H}_2\text{O})$ products (Fig. 4). See <http://www.rsc.org/suppdata/jm/b1/b106734f/>

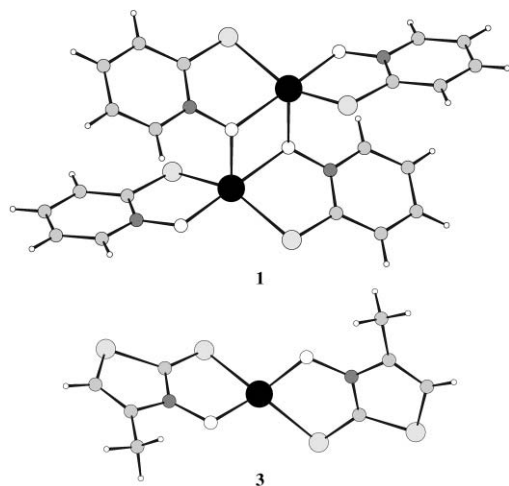


Fig. 1 Molecular structures of **1** and **3** in the solid state.

attributed to chelate complex formation,¹⁴ and we have, therefore, been studying other cyclic thiohydroxamic acids with similar chelating groups. One such molecule is 3-hydroxy-4-methyl-2(3*H*)-thiazolethione (HMTT).¹⁵ We have reported previously the solid-state structures of several divalent complexes of HMTT with d-block elements, including that of Zn(MTT)₂ **3**.^{16–18} We report here the synthesis and characterisation of a mixed-molecular material incorporating both the PT and MTT units as part of a hydrated zinc complex. Extensive crystallographic disorder prohibits unambiguous identification of the molecular components present in the material, but additional evidence suggests that the hydrate Zn(MTT)₂(H₂O) **4** is *not* present. Instead, the mixed molecule Zn(PT)(MTT)(H₂O) **5** is formed and this forms a continuous solid solution with **2** over the entire composition range.

Results and discussion

Molecular modelling: prospects for solid-solution formation

To a first approximation, the prospects for solid-solution formation between two molecular components may be assessed in terms of their shape and size. This may be quantified by the coefficient of geometric similarity, ϵ ,

$$\epsilon = 1 - R/r$$

where R is the volume of non-overlapping parts and r is the volume of overlapping parts when the two molecules are overlaid.⁷ The generally accepted minimum value of ϵ required for significant solubility is 0.8. Although **1** and **3** have largely similar molecular structures, prospects for the formation of mixed crystals seem slight since the two complexes adopt vastly different structures in the solid state: **1** forms dimeric units in which zinc adopts 5-coordination, whereas **3** remains monomeric with a tetrahedral zinc centre (Fig. 1).^{12,17} ‡ Dimerisation of **1** may be avoided, however, by formation of the hydrate **2**, and comparison of this molecule with a hypothetical analogous Zn(MTT)₂ hydrate **4** suggests that these two molecules may possess suitable geometries for solid-solution formation; ϵ for the two molecules is 0.93, well above the limiting value for solubility (Fig. 2). Thus it may be envisaged that molecules of **4** may be inserted into a lattice of **2** with minimal disruption.

A more stringent criterion for assessing the prospects of solid-solution formation is the enthalpy change resulting from incorporation of the solute (the minor component) into the lattice of the solvent (the major component). This may be

‡ Dimerisation of **2** is prohibited by the steric influence of the methyl substituent in MTT.

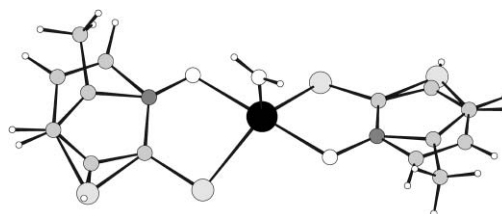


Fig. 2 Molecules of the hydrates **2** and **4** overlaid: $\epsilon = 0.93$.

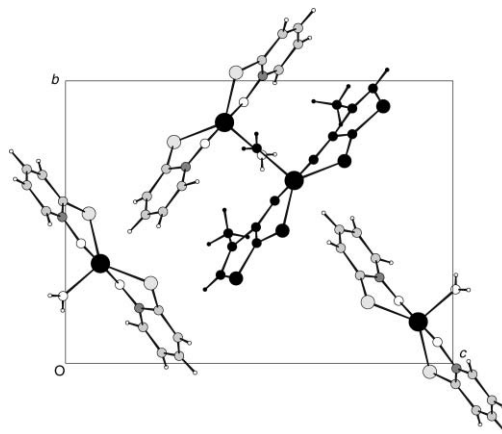


Fig. 3 Model of a unit cell of **2** with one molecule of **2** replaced by **4** (shaded black) corresponding to 25% substitution.

Table 1 Calculated lattice binding energies and unit-cell parameters for energy minimised models^a of a solid solution of **2** and **4**: Zn(PT)_{*x*}(MTT)_{2–*x*}(H₂O)

<i>x</i>	$E_{\text{latt}}/\text{kJ mol}^{-1}$	<i>a</i> /Å	<i>b</i> /Å	<i>c</i> /Å	<i>V</i> /Å ³
0	–191.1	7.670	11.538	15.648	1384.8
0.25	–199.9	7.172	11.761	16.553	1396.2
0.50	–199.5	7.222	11.752	16.427	1394.2
0.75	–198.5	7.290	11.716	16.268	1389.4
1.00	–195.5	7.484	11.650	16.059	1400.2
1.25	–195.5	7.540	11.613	15.929	1394.8
1.50	–194.2	7.590	11.622	15.782	1392.1
1.75	–194.0	7.644	11.551	15.742	1390.0
2.00	–201.4	7.005	11.824	15.811	1309.6

^aUnit-cell parameters minimised within the constraints of the orthorhombic crystal system, *i.e.* $\alpha = \beta = \gamma = 90^\circ$.

assessed by calculation of lattice binding energies *via* the atom–atom method. Models of a solid solution of **2** and **4** may be generated by substituting molecules of **4** in the structure of **2**, simply by replacing the PT ligands with MTT ligands. Replacing one molecule per unit cell (space group $P2_12_12_1$, $Z=4$) corresponds to 25% substitution; two molecules corresponds to 50% substitution, *etc.* (Fig. 3) Intermediate levels of substitution may be modelled by constructing a superstructure in the space group $P1$ from a number of unit cells. The substitution is not truly random since the finite size of the model introduces some degree of order; this may be minimised by increasing the size of the superstructure, but with a corresponding computational cost. Models were constructed in this case for the range of solution compositions available from a superstructure of two unit cells. The models were subjected to lattice-energy minimisation with the results listed in Table 1.

Over the entire composition range, the calculated lattice binding energy changes by *ca.* 10.3 kJ mol^{–1}, considerably less than that reported in similar studies where solid-solution formation has been observed.⁸ On incorporation of **4** into a lattice of **2**, the structure initially becomes less stable with an increase in unit-cell volume (as would be expected for

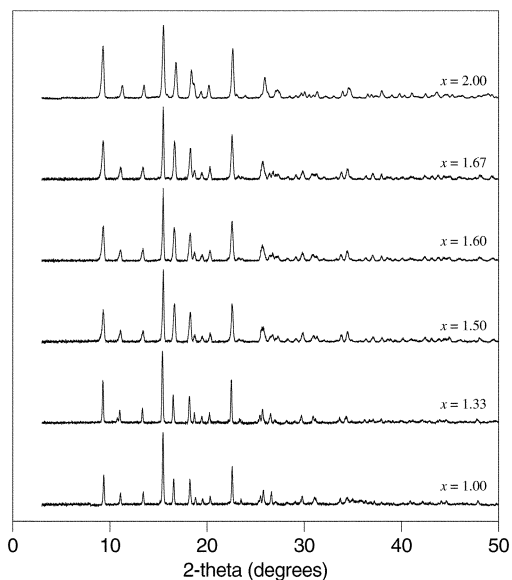


Fig. 4 PXRD profiles for the single phase $\text{Zn}(\text{PT})_x(\text{MTT})_{2-x}(\text{H}_2\text{O})$ products. The $x=2$ product corresponds to $\text{Zn}(\text{PT})_2(\text{H}_2\text{O})$ **2**. The $x=1$ product was synthesised at reduced temperature in DMF. Lists of reflection indices and refined lattice parameters are available as ESI.†

incorporation of the larger molecule **4**) then becomes gradually more stable with further substitution, with little change in unit-cell volume. The $x=0$ case, corresponding to pure **4**, is calculated to be considerably less stable than the $x=0.25$ model. From the relatively small changes in the calculated lattice binding energies and unit-cell volumes, it may be expected that **2** and **4** will form a solid solution over a considerable composition range.

Synthesis of $\text{Zn}(\text{PT})_x(\text{MTT})_{2-x}(\text{H}_2\text{O})$

Bulk samples of the solid solution $\text{Zn}(\text{PT})_x(\text{MTT})_{2-x}(\text{H}_2\text{O})$ were prepared by stirring mixtures of **1** and **3** [in a ratio $x:(2-x)$ for $x=0.33, 0.40, 0.50, 0.67, 1.00, 1.33, 1.50, 1.60, 1.67$] in *ca.* 10 ml dimethylsulfoxide (DMSO), followed by rapid addition of *ca.* 100 ml water at room temperature. The resulting white precipitates were filtered under gravity and dried in air. For all samples with $x>1$, PXRD profiles indicated formation of identical phases, and comparison with the PXRD profile of $\text{Zn}(\text{PT})_2(\text{H}_2\text{O})$ **2** showed that the phases are isostructural with **2** (Fig. 4). The stoichiometries were confirmed as $\text{Zn}(\text{PT})_x(\text{MTT})_{2-x}(\text{H}_2\text{O})$ by elemental and thermogravimetric analyses (Table 2). For the equimolar sample ($x=1$), and for all samples with $x<1$, mixed phases were formed: peaks corresponding to **3** were also observed in the PXRD profiles in addition to those of the $\text{Zn}(\text{PT})_x(\text{MTT})_{2-x}(\text{H}_2\text{O})$ phase. At low temperature (*ca.* 3 °C), using *N,N*-dimethylformamide (DMF) as the solvent (since DMSO freezes at 18 °C), a single phase of stoichiometry $\text{Zn}(\text{PT})(\text{MTT})(\text{H}_2\text{O})$ was produced, isostructural with the

Table 2 Elemental analyses, thermogravimetric analyses and melting points for $\text{Zn}(\text{PT})_x(\text{MTT})_{2-x}(\text{H}_2\text{O})$ with $1 \leq x \leq 2$

x	C (%)	H (%)	N (%)	Mass loss 25–200 °C (%) ^a	Mp/°C
1.00	30.7 (30.4)	2.9 (2.8)	7.9 (7.9)	5.1 (5.1)	211–212
1.33	32.1 (32.1)	2.9 (2.9)	8.0 (8.0)	5.1 (5.2)	211–212
1.50	33.1 (33.0)	2.9 (2.9)	7.9 (8.1)	5.3 (5.2)	213–214
1.60	33.6 (33.5)	2.9 (2.9)	7.9 (8.1)	5.2 (5.3)	236–238
1.67	33.7 (33.9)	3.0 (2.9)	7.9 (8.2)	5.3 (5.3)	242–244
2.00	35.7 (35.8)	3.0 (3.0)	8.3 (8.3)	5.2 (5.4)	258–260

^aMass loss corresponds to loss of water. Figures in parentheses denote values calculated from proposed formulae.

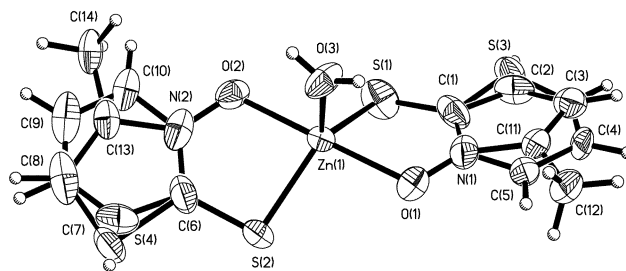


Fig. 5 Asymmetric unit in the refined crystal structure of $\text{Zn}(\text{PT})_{1.2}(\text{MTT})_{0.8}(\text{H}_2\text{O})$ at 150(2) K, with displacement ellipsoids at 50% probability.

previous $\text{Zn}(\text{PT})_x(\text{MTT})_{2-x}(\text{H}_2\text{O})$ phases (Fig. 4). Elemental and thermogravimetric analyses confirm the stoichiometry of this product (Table 2). All samples with $x<1$ continue to form mixtures containing **3** at low temperature, suggesting that the lower limit for x is unity. The formation of **2** sets the upper limit for x as 2. Thus, the entire series of materials may be represented as $\text{Zn}(\text{PT})_x(\text{MTT})_{2-x}(\text{H}_2\text{O})$, with $1 \leq x \leq 2$. Application of the synthesis procedure using **3** as the sole reactant did not produce the hydrate **4**; **3** was precipitated at all temperatures employed.

Single-crystal X-ray diffraction

Diffraction data were collected from a single crystal obtained by slow evaporation of an equimolar solution of **1** and **3** in a dimethylsulfoxide (DMSO)–water mixture. § Structure solution located initially a central ZnS_2O_3 unit with a PT ligand on one side and an MTT ligand on the other. Subsequent Fourier syntheses located a PT ligand at the side occupied by MTT in the initial model, and an MTT ligand at the side occupied by PT. Thus, the asymmetric unit contains an ordered ZnS_2O_3 unit on a single lattice site with a disordered mixture of PT and MTT ligands on each side (Fig. 5). The molecular unit has *pseudo-C*₂ point symmetry with the two-fold axis lying along the Zn–(OH)₂ bond. In view of the disordered nature of the structure, X-ray data were collected from the same crystal cooled to 150(2) K; low-temperature data collection minimises dynamic disorder and often facilitates interpretation of static disorder. Subsequent refinement was performed against the 150(2) K data set. The disorder remains complex even at reduced temperature. The possibility of incorrect assignment of the unit cell (*e.g.* halving of a unit-cell axis) may be discounted since images from the CCD detector allow for a rapid visual search for additional unindexed reflections – none were observed.

In order to proceed with refinement of a structure where such complex disorder exists, it is prudent to employ suitable constraints and restraints. In this case, it is essential to consider carefully the validity of each proposed constraint. It should not be assumed, for example, that the PT and MTT ligands are present in the crystal in a 1 : 1 ratio. Although the solution from which the crystal was obtained contained an equimolar ratio of PT and MTT, the individual crystal selected need not. At each side of the ZnS_2O_3 unit, there *must* be either a PT ligand or an MTT ligand so that the site occupancies of the PT and MTT ligands on a given side of the ZnS_2O_3 unit must sum to unity. Thus, the following constraint was employed: $(\text{PT})_k(\text{MTT})_l - \text{Zn}(\text{OH})_2 - (\text{PT})_m(\text{MTT})_n$; $k+l=1$ and $m+n=1$. In addition, it is reasonable to assume that the chemically-equivalent PT and MTT ligands at each end of the molecule have comparable geometries. This observation was treated by restraining equivalent bond distances in the PT and MTT ligands to be

§**1** and **3** were dissolved in DMSO, and water was added dropwise until the first signs of precipitation. Further DMSO was then added dropwise until the precipitate was fully redissolved.

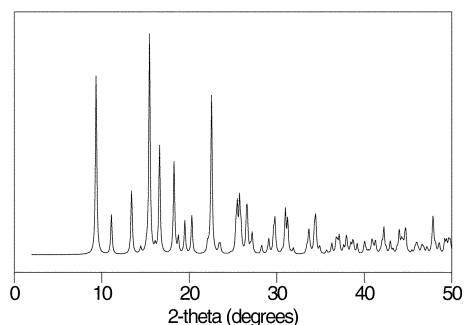
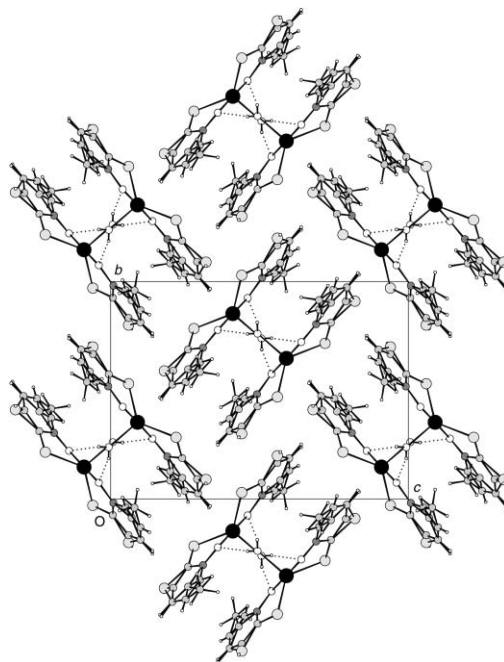
Table 3 Crystallographic data for $\text{Zn}(\text{PT})_{1.2}(\text{MTT})_{0.8}(\text{H}_2\text{O})$, ($x=1.2$)

Empirical formula	$\text{C}_{9.2}\text{H}_{10}\text{N}_2\text{O}_3\text{S}_{2.8}\text{Zn}$
M	351.73
Crystal system	Orthorhombic
Space group	$P2_12_12_1$
$a/\text{\AA}$	7.1353(5)
$b/\text{\AA}$	11.6238(5)
$c/\text{\AA}$	15.9011(12)
$V/\text{\AA}^3$	1318.8(2)
T/K	150(2)
Z	4
$D_c/\text{g cm}^{-3}$	1.771
$\mu(\text{Mo K}\alpha)/\text{mm}^{-1}$	2.305
Total data	5887
Unique data	2313
Observed data [$F^2 > 2\sigma(F^2)$]	2176
R_{int}	0.037
$R1$ [$F^2 > 2\sigma(F^2)$]	0.027
$wR2$ [$F^2 > 2\sigma(F^2)$]	0.055
Goodness of fit on F^2 , S	1.085
Absolute structure parameter	0.002(14)

the same with a standard deviation of 0.01 Å, and equivalent 1,3-distances to be the same with a standard deviation of 0.02 Å. These 'similarity restraints' equalise distances which are chemically equivalent but not crystallographically equivalent, without introducing any artificial values.¹⁹

Initially, the site occupancy factors of the PT and MTT ligands were set at 0.5 (*i.e.* $k=l=m=n=0.5$). The positions of all the atoms in the central ZnS_2O_3 unit were refined with full site occupancy and anisotropic displacement parameters, while the remaining atoms were refined with isotropic displacement parameters. The similarity restraints were employed as described. Site occupancy factors for the PT and MTT ligands were then refined with fixed isotropic displacement parameters and the constraints described previously. N(1), C(1), C(3), N(2), C(6) and C(8) were each split into two atoms forming part of the PT and MTT ligands, respectively. It was found that the two parts of each of these split atoms remained at the same positions and they were subsequently constrained as such; in this manner, N(1), C(1), C(3), N(2), C(6) and C(8) are full-occupancy atoms common to both the PT and MTT ligands. The refinement converged to give: $(\text{PT})_k(\text{MTT})_l\text{-Zn}(\text{OH}_2)\text{-}(\text{PT})_m(\text{MTT})_n$; $k=m=0.60(1)$; $l=n=0.40(1)$. Thus, the composition of the crystal analysed is $\text{Zn}(\text{PT})_{1.2}(\text{MTT})_{0.8}(\text{H}_2\text{O})$. In subsequent cycles of refinement, the site occupancy factors were fixed at these values and all atoms were refined with anisotropic displacement parameters. The crystallographic data are summarised in Table 3 and the asymmetric unit showing displacement ellipsoids is illustrated in Fig. 5. Comparison of a powder X-ray diffraction profile simulated from the single crystal structure with that of the bulk $\text{Zn}(\text{PT})_x(\text{MTT})_{2-x}(\text{H}_2\text{O})$ samples confirms that the single crystal structure is representative (Fig. 6).

Molecules are linked *via* O–H...O hydrogen bonds into chains running along the a direction (Fig. 7). The PT and MTT

**Fig. 6** Simulated PXRD profile from the single-crystal structure of $\text{Zn}(\text{PT})_{1.2}(\text{MTT})_{0.8}(\text{H}_2\text{O})$.**Fig. 7** View along the a direction of the crystal structure of $\text{Zn}(\text{PT})_{1.2}(\text{MTT})_{0.8}(\text{H}_2\text{O})$.

ligands of molecules adjacent in the chains adopt an approximate co-planar arrangement (interplane angle 2.8°) with a separation of 3.44 Å between the least-squares planes through the pyridine and thiazole rings of the PT and MTT ligands, respectively. Owing to the complex disorder of the system, it is not possible on the basis of the crystallographic evidence alone to state whether PT ligands are brought into face-to-face contact with other PT ligands or with MTT ligands.

Interpretation of the refined structure model

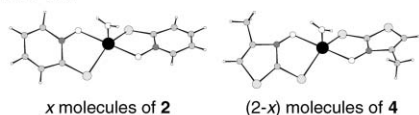
As a result of the complex disorder, the refined model from the single-crystal X-ray analysis does not allow unambiguous identification of the molecular species. The most straightforward interpretation is that proposed initially, namely that the crystal comprises molecules of **2** and **4** disordered randomly over the lattice sites.¶ Each lattice site is occupied by *either 2 or 4* with an overall 60:40 ratio of the two species (model A; Scheme 1). For the general case, $\text{Zn}(\text{PT})_x(\text{MTT})_{2-x}(\text{H}_2\text{O})$, **2** and **4** are present in the ratio $x:(2-x)$.

A second interpretation of the model may also be postulated, however, which includes the mixed molecule $\text{Zn}(\text{PT})(\text{MTT})(\text{H}_2\text{O})$ **5** – this may arise at the point of synthesis as a result of ligand exchange in DMSO or DMF solution. Orientational disorder of this molecule about the (non-crystallographic) two-fold axis through the Zn(1)–O(3) bond gives rise to the observed asymmetric unit. For the $x=1$ material, complete randomisation over the two orientations would result in site occupancy factors of 0.5 for the PT and MTT ligands. *Non-random* disorder could result in a site occupancy factor greater than 0.5 for the PT ligand on one side of the ZnS_2O_3 unit, but this must be accompanied by the corresponding site occupancy factor less than 0.5 for the other PT ligand. Observation of site occupancy factors greater than 0.5 for the PT ligand on *both* sides of the ZnS_2O_3 unit suggests that additional molecules of **2** must be present in the crystal analysed ($x=1.2$). Thus, the second description of the structure involves a solid solution of **2** in a lattice of **5**, with the molecules of **5** disordered randomly over two orientations related by the

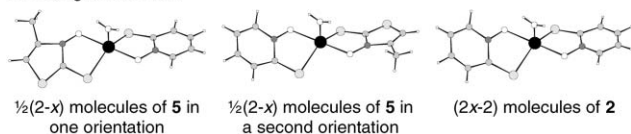
¶Although **4** has not been prepared in isolation, this does not preclude its presence in the solid solution with **2**.

Model A

On a single lattice site:

**Model B**

On a single lattice site:

**Scheme 1** Alternative interpretations of the refined structure model from the single-crystal X-ray analysis of $\text{Zn}(\text{PT})_x(\text{MTT})_{2-x}(\text{H}_2\text{O})$.

pseudo-two-fold axis (model **B**; Scheme 1). In the crystal analysed, this corresponds to 80% **5** and 20% **2**. For the general case, $\text{Zn}(\text{PT})_x(\text{MTT})_{2-x}(\text{H}_2\text{O})$, (2-x) molecules of **5** are disordered randomly over two orientations with (2x-2) molecules of **2** also present.

It should be noted that whichever interpretation of the model is chosen, molecules of **2** *must* be present where $x > 1$; the same conclusion does not necessarily apply for **4**. Since the X-ray diffraction technique samples long-range structure, it is not possible to distinguish between models **A** and **B** on the basis of the X-ray data alone. Furthermore, it is not possible to determine whether the disorder is entirely random; in the first case, for example, there may be clusters of **2** and **4** within the crystal. In the extreme, crystals of the two different species may be intimately fused. Further characterisation techniques are required therefore to elucidate the nature of the molecular species in $\text{Zn}(\text{PT})_x(\text{MTT})_{2-x}(\text{H}_2\text{O})$.

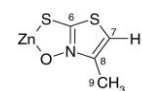
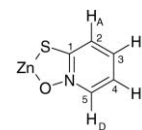
Further characterisation of $\text{Zn}(\text{PT})_x(\text{MTT})_{2-x}(\text{H}_2\text{O})$

^1H and ^{13}C solution NMR. Characterisation of $\text{Zn}(\text{PT})_x(\text{MTT})_{2-x}(\text{H}_2\text{O})$ depends ultimately upon identification of the species present in the complex with $x=1$. Of course, the mixed molecule **5** can only be present in the first instance if ligand exchange is possible in DMSO and DMF solution. If ligand exchange were not possible, model **B** could be discounted immediately. To investigate the prospect of ligand exchange, ^1H and ^{13}C NMR spectra were acquired for **1**, **3** and an equimolar physical mixture of the two components, in d_6 -DMSO solutions. The chemical shifts and peak assignments are listed in Table 4. The spectrum of the physical mixture is simply a superposition of the spectra of **1** and **3**. This may be interpreted in three ways. First, ligand exchange is not occurring. Second, ligand exchange is occurring, but the chemical shifts in the mixed molecule $\text{Zn}(\text{PT})(\text{MTT})$ are indistinguishable from those in **1** and **3**. Third, ligand exchange is occurring, but at a rate sufficiently rapid that any differences in the spectrum resulting from the presence of the mixed molecule are time-averaged. These three cases cannot be distinguished, and little information can be deduced from the solution NMR spectra.

Mass spectrometry. It is necessary to distinguish between the mixed molecule **5** disordered equally over two orientations, and an equimolar solid solution of **2** and **4**. A suitable technique must clearly be a solid-state one since dissolution of the samples may lead to further ligand exchange. Mass spectrometry is perhaps the most obvious possibility, since the mass of the mixed molecule will clearly be different from the masses of the other two species. Any MS technique that requires dissolution of the sample prior to vaporisation is not suitable. **1** and **3** were, therefore, vaporised directly from the solid state by electron impact, and peaks corresponding to the ions $\text{Zn}(\text{PT})_2^+$ and $\text{Zn}(\text{MTT})_2^+$ are observed at m/z 316 and 356,

Table 4 Chemical shifts (relative to TMS) and peak assignments for the ^1H and ^{13}C solution NMR analyses of **1**, **3** and an equimolar physical mixture of the two components

	δ/ppm (^1H)		δ/ppm (^{13}C)	
1	6.97 (t, 1H)	H_C	159.56	C(1)
	7.22 (t, 1H)	H_B	137.41	C(5)
	7.58 (d, 1H)	H_A	129.46	C(2)
	8.41 (d, 1H)	H_D	128.52	C(3)
			117.96	C(4)
3	2.28 (s, 3H)	Methyl	158.09	C(6)
	6.99 (s, 1H)	H_E	140.48	C(8)
			105.07	C(7)
			14.27	C(9)
1+3	2.28 (s, 3H)	Methyl	159.53	C(1)
	6.98 (m, 2H)	H_C , H_E	157.92	C(6)
	7.22 (t, 1H)	H_B	140.14	C(8)
	7.58 (d, 1H)	H_A	137.41	C(5)
	8.41 (d, 1H)	H_D	129.42	C(2)
			128.53	C(3)
			117.98	C(4)
			104.51	C(7)
			13.89	C(9)



respectively. A physical mixture of **1** and **3** was also prepared by shaking equimolar amounts of the two materials. The same peaks are observed in the spectrum of the mixture, but an additional peak arises at m/z 336 corresponding to the ion of the mixed material, $\text{Zn}(\text{PT})(\text{MTT})^+$. Thus, ligand exchange occurs at some stage within the instrument, prohibiting the use of mass spectrometry to distinguish between the models **A** and **B**.

High-temperature powder X-ray diffraction (PXRD). We have shown previously that on dehydration, **2** reverts to dimeric **1**.¹³ For all $\text{Zn}(\text{PT})_x(\text{MTT})_{2-x}(\text{H}_2\text{O})$ with $x > 1$, molecules of **2** *must* be present regardless of whichever model (**A** or **B**) is the correct one. Thus, it might be expected that on dehydration, some dimeric **1** will be formed from all $\text{Zn}(\text{PT})_x(\text{MTT})_{2-x}(\text{H}_2\text{O})$ with $x > 1$. PXRD data for $\text{Zn}(\text{PT})_{1.33}(\text{MTT})_{0.67}(\text{H}_2\text{O})$ were collected at 100 °C and the profile obtained does indeed show peaks corresponding to dimeric **1** and also peaks indicative of a structure similar to that of **3** (Fig. 8). It may *not* be stated conclusively, however, that the second phase is **3** itself (which would indicate model **A**) since the mixed molecule **5** might also adopt a structure similar to that of **3**. The dimeric $\text{Zn}(\text{PT})_2$ structure type, however, cannot be anything other than **1** since steric effects prohibit incorporation of the MTT ligand in this structure.

The key compound for distinguishing between models **A** and **B** is, of course, the $x=1$ material. Dehydration of model **A** would be expected to produce a mixture of **3** and dimeric **1**. Dehydration of model **B** would be expected to leave a single phase **5** which is likely to adopt a structure similar to that of **3**. The PXRD pattern of $\text{Zn}(\text{PT})(\text{MTT})(\text{H}_2\text{O})$ measured at 100 °C indicates an essentially pure phase with a structure similar to that of **3** (Fig. 9). Peaks corresponding to dimeric **1** are present but with intensities indicative of a very minor constituent. This is likely to be a result of excess **1** introduced during synthesis (*i.e.* for the material examined x is slightly greater than

1 and **3** were ground separately then combined by shaking since grinding the two components *together* may initiate ligand exchange (although grinding experiments performed in the course of this work indicate that this does not occur).

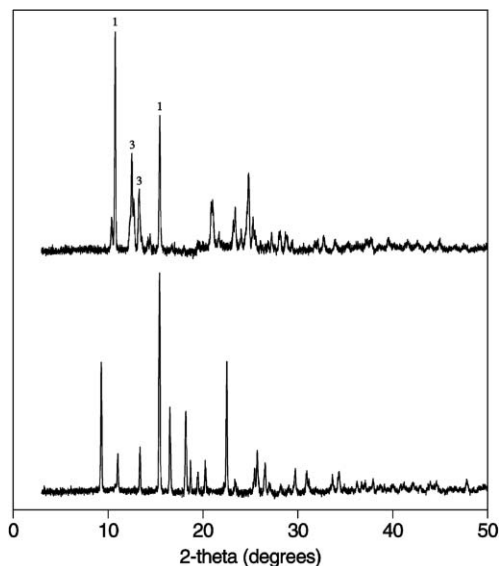


Fig. 8 PXRD profile of $\text{Zn}(\text{PT})_{1.33}(\text{MTT})_{0.67}(\text{H}_2\text{O})$ at room temperature (bottom) and at 100°C (top). Peaks marked 1 and 3 correspond to the most intense peaks in the PXRD profiles of **1** and **3**, respectively.

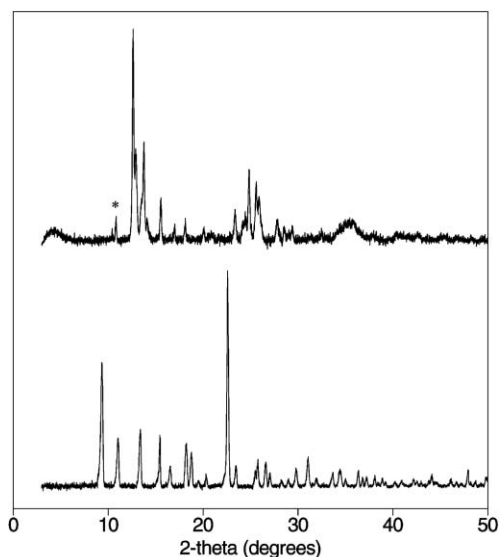


Fig. 9 PXRD profile of $\text{Zn}(\text{PT})(\text{MTT})(\text{H}_2\text{O})$ at room temperature (bottom) and at 100°C (top). Peaks marked with an asterisk correspond to a minor component **1**.

unity).** The major phase, therefore, has stoichiometry $\text{Zn}(\text{PT})(\text{MTT})$ and a structure similar to that of **3**. The fact that dimeric **1** is observed on dehydration of all $\text{Zn}(\text{PT})_x(\text{MTT})_{2-x}(\text{H}_2\text{O})$ with $x > 1$ and *not* observed to any great extent in this case suggests that **2** is not present in the $x = 1$ material, *i.e.* model **B** is the correct one.

Solid-state ^{13}C NMR. ^1H - ^{13}C CP/MAS NMR spectra were acquired for freshly-synthesised samples of **1**, **2** and $\text{Zn}(\text{PT})(\text{MTT})(\text{H}_2\text{O})$. PXRD analysis of the samples prior to acquisition of the NMR spectra confirmed that they were pure phases. The chemical shifts, peak assignments and aromatic

Incorporation of excess **1 may arise as a result of its greater solubility in DMF compared with **3**. For synthesis of the $x = 1$ material, equimolar amounts of **1** and **3** are stirred initially in DMF and the solution is filtered to remove any minor insoluble impurities prior to the addition of water. At this stage, any undissolved starting material will also be removed. The greater solubility of **1** means that any starting material which might be removed is more likely to be **3**, thus leaving a slight excess of **1**.

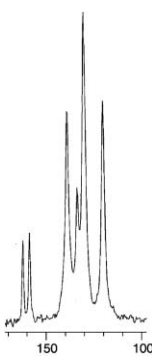
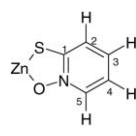
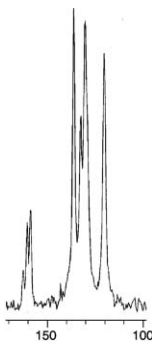
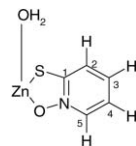
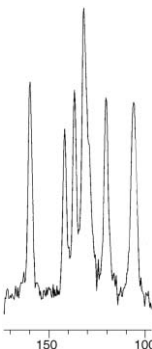
regions of the spectra are given in Table 5. The most significant differences between the spectra are observed in the 159–163 ppm region. In **2**, the peak at 160.8 ppm may be assigned to C(1). In **1**, two peaks arise at 158.9 and 162.4 ppm, assigned to C(1) in two different chemical environments in the $[\text{Zn}(\text{PT})_2]_2$ dimer. Peaks also arise at 159.1 and 162.8 ppm in **2**, indicating the presence of some anhydrous **1** in the hydrate sample. This impurity may arise either at the point of synthesis or from dehydration of the hydrate. Since PXRD analysis of the sample prior to acquisition of the NMR data suggested that the phase **2** was pure, the latter explanation is more probable. In $\text{Zn}(\text{PT})(\text{MTT})(\text{H}_2\text{O})$, a single peak is observed at 160.2 ppm for C(1) [also assigned to C(6)], indicating that the anhydrous **1** impurity is not present in this sample. The fact that dehydration to form $\text{Zn}(\text{PT})_2$ does not occur for $\text{Zn}(\text{PT})(\text{MTT})(\text{H}_2\text{O})$ suggests that $\text{Zn}(\text{PT})_2(\text{H}_2\text{O})$ is not present. Thus, the solid-state NMR data are also consistent with model **B**.

A further difference between the spectra of $\text{Zn}(\text{PT})(\text{MTT})(\text{H}_2\text{O})$ and **2** arises in the 120–145 ppm region. In **2**, four distinct peaks are observed. In $\text{Zn}(\text{PT})(\text{MTT})(\text{H}_2\text{O})$, the two central peaks of this group [assigned to C(2) and C(3)] are merged into a single peak with a slight shoulder. The change in chemical shift for carbons C(2) and C(3) of the pyriothione ring in $\text{Zn}(\text{PT})(\text{MTT})(\text{H}_2\text{O})$ indicates a change in their chemical environments compared with those in **2**. This does not actually assist with identification of the molecular species since it is most likely to reflect a change in the intermolecular environment – it is unlikely that the chemical shifts of C(2) and C(3) are sensitive to the identity of the ligand at the opposite end of a single molecule since they are so far removed in space. The change in the spectrum does suggest, however, that PT rings in $\text{Zn}(\text{PT})(\text{MTT})(\text{H}_2\text{O})$ adopt positions adjacent to MTT rings in neighbouring molecules rather than PT rings (Fig. 10). It is not possible to examine comparable changes in the chemical shifts of carbons in MTT as a result of changes in intermolecular environment since **4** cannot be prepared.

Modelling of the proposed structure

Modelling of a solid solution of **2** in **5** may be achieved in a manner similar to that described previously. The coefficient of geometrical similarity for **2** and **5** is 0.97, even greater than that for **2** and **4** since one half of each molecule is now identical – the prospects of solid-solution formation for these two molecules are therefore even greater than those of **2** and **4**. One additional piece of information which may be derived from modelling the $x = 1$ solid solution involves clarification of the arrangement of the mixed molecule within the hydrogen-bonded chains: is the structure stabilised by bringing PT ligands into face-to-face contact with MTT ligands (as suggested by the solid-state NMR data), or is the structure more stable with only PT–PT and MTT–MTT contacts? It is possible to arrange the molecules within the hydrogen-bonded chains in either of these arrangements and still give rise to the observed disorder. Models were prepared for each situation and energy minimisation resulted in calculated lattice binding energies of -209.16 and -204.31 kJ mol^{-1} for the two cases, respectively. This suggests, therefore, that the structure is stabilised by bringing PT and MTT ligands into face-to-face contact only with ligands of the opposite type, consistent with the proposal made on the basis of the solid-state NMR evidence. The fact that **2** may be prepared indicates that PT–PT face-to-face contacts are not destabilising within the structure and suggests therefore that MTT–MTT contacts might be. This observation is consistent with the fact that solid solutions with $x < 1$ cannot be prepared; these would necessarily contain some destabilising MTT–MTT contacts. The destabilising nature of these contacts may be a result of the steric influence of the methyl substituents.

Table 5 Aromatic regions of the ^1H - ^{13}C CP/MAS solid-state NMR spectra, chemical shifts (relative to TMS) and peak assignments for **1**, **2** and $\text{Zn}(\text{PT})(\text{MTT})(\text{H}_2\text{O})$

	δ/ppm			
1		120.5	C(4)	
		130.5	C(3)	
		133.9	C(2)	
		139.2	C(5)	
		158.9	C(1)	
		162.4	C(1')	
2		120.7	C(4)	
		130.7	C(3)	
		133.0	C(2)	
		136.6	C(5)	
		160.8	C(1)	
		159.1	^a	
		162.8	^b	
		$\text{Zn}(\text{PT})(\text{MTT})(\text{H}_2\text{O})$		
120.6	C(4)			
132.2	C(2), C(3)			
137.1	C(5)			
142.2	C(8)			
160.2	C(1), C(6)			

^aC(1) from $\text{Zn}(\text{PT})_2$ impurity. ^bC(1') from $\text{Zn}(\text{PT})_2$ impurity.

Conclusions

It may be concluded with certainty that the series of compounds $\text{Zn}(\text{PT})_x(\text{MTT})_{2-x}(\text{H}_2\text{O})$ with $1 \leq x \leq 2$ incorporate

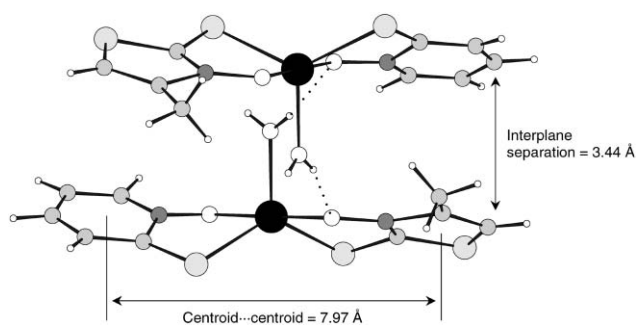


Fig. 10 Adjacent molecules in chains of $\text{Zn}(\text{PT})(\text{MTT})(\text{H}_2\text{O})$, indicating the spatial separation between PT and MTT ligands in the same molecule. Much closer contacts are evident *between* molecules

both the fungicidal pyriothione (PT) and methylthiazolethione (MTT) moieties. No single technique considered here, however, facilitates conclusive distinction between the mixed molecule $\text{Zn}(\text{PT})(\text{MTT})(\text{H}_2\text{O})$ **5** and a mixture of $\text{Zn}(\text{PT})_2(\text{H}_2\text{O})$ **2** and $\text{Zn}(\text{MTT})_2(\text{H}_2\text{O})$ **4** in the solid state. The PXRD evidence strongly suggests that $\text{Zn}(\text{PT})_x(\text{MTT})_{2-x}(\text{H}_2\text{O})$ contains the mixed molecule **5**, and this proposal is supported by solid-state ^1H - ^{13}C CP/MAS NMR. Further supporting evidence is provided indirectly by the observation that the minimum limit of x in $\text{Zn}(\text{PT})_x(\text{MTT})_{2-x}(\text{H}_2\text{O})$ is unity. If the mixed crystals were solid solutions of **2** and **4**, there is no obvious explanation as to why the two components should abruptly become insoluble at the $x=1$ limit; calculation of the lattice binding energies of solid solutions of **2** and **4** suggest that they should be stable over the entire composition range. To date it has not been possible to prepare the hydrate **4** under any conditions. Crystallisation of **3** from DMSO-water mixtures (thermodynamic control) yields only crystals of **3**. Rapid quenching of DMF solutions of **3** by addition of water at

reduced temperature (kinetic control) also yields only **3**. In all $\text{Zn}(\text{PT})_x(\text{MTT})_{2-x}(\text{H}_2\text{O})$ syntheses with $x < 1$, anhydrous **3** is observed in addition to the desired mixed-crystal hydrate. This suggests therefore that **4** cannot be prepared under the conditions of the $\text{Zn}(\text{PT})_x(\text{MTT})_{2-x}(\text{H}_2\text{O})$ syntheses, adding further weight to the selection of model **B**. This may be a result of destabilising face-to-face MTT–MTT contacts within the crystal structure. With the conclusion that the $x = 1$ material contains the mixed molecule **5**, the dehydration product of **5** must then be the novel anhydrous mixed material $\text{Zn}(\text{PT})(\text{MTT})$. The PXRD profile of this material shows it to be isostructural with **3**. As for **3** itself, the solid-state structure contains tetrahedral monomeric units rather than the dimers observed in **2**; this may be attributed to the steric influence of the methyl substituent in the MTT ligand.

Experimental

Molecular modelling

All molecular modelling procedures were performed using the Cerius² package (ver. 4.0).²⁰ For the energy minimisations, the generic force field Dreiding was employed with default parameters²¹ and the Ewald summation technique was employed to accelerate convergence of the electrostatic terms.²² Partial atomic charges were derived from the electrostatic potential calculated using the MOPAC semi-empirical molecular orbital program using the AM1 model;^{23,24} these have been shown to be superior for general organic molecules and it has also been our experience that they are suitable for treatment of metallo-organic complexes.²⁵ Minimisation was performed initially using rigid molecular units free to rotate and translate within a fixed unit cell. In a subsequent minimisation step, unit-cell parameters were also relaxed within the constraints of the crystal system. To assess the suitability of the Dreiding force field and the model of the atomic charges, the experimentally-determined crystal structure of **2** [$a = 7.119(3)$, $b = 11.897(5)$, $c = 15.588(10)$ Å] was subjected to rigid-body minimisation in the manner described. The final minimised model has $E_{\text{latt}} = -201.4$ kJ mol⁻¹ with unit-cell parameters $a = 7.005$, $b = 11.824$, $c = 15.811$ Å. The mean change in cell lengths of 0.137 Å (maximum change of 0.223 Å in c) is small and indicates that the force field provides an adequate empirical description of the intermolecular interactions.

Single-crystal X-ray diffraction

Single-crystal X-ray diffraction analyses were performed on a Nonius KappaCCD diffractometer using graphite-monochromated Mo K α radiation ($\lambda = 0.7107$ Å). Lattice parameters were determined from 10 frames recorded with 1° ϕ scans and subsequently refined against all data. Data were collected using 2° ω and ϕ scans with an exposure time of 240 s per frame and the crystal-to-detector distance fixed at 35 mm. The data were processed using the HKL package²⁶ and a multi-scan absorption correction was applied using SORTAV.²⁷ The structure was solved by direct methods using SIR-92²⁸ and refined on F^2 using SHELXL-97.²⁹ Hydrogen atoms bound to carbon were placed geometrically and allowed to ride during subsequent refinement with an isotropic displacement parameter fixed at 1.2 times U_{eq} for the carbon to which they are attached. Hydrogens on the water molecule were located in a difference Fourier map and refined with an isotropic displacement parameter and the O(3)–H bond distance restrained to 0.82(2) Å (derived from the SHELXL default distance at 150 K).

CCDC reference number 168321.

See <http://www.rsc.org/suppdata/jm/b1/b106734f/> for crystallographic data in CIF or other electronic format.

Powder X-ray diffraction (PXRD)

PXRD analyses were performed on a Stoe STADI-P high-resolution laboratory diffractometer using Ge(111)-monochromated Cu K α radiation ($\lambda = 1.5406$ Å) and a position-sensitive detector (PSD) covering approximately 6° in 2θ . Patterns were measured in transmission geometry using an ω - 2θ scan technique over the range $3 \leq 2\theta \leq 50^\circ$, with a step size of 2.5° and a count time of 360 s per step. Data were collected from finely-ground samples rotated about the normal to the plane of the sample in order to minimise preferred orientation effects.

Nuclear magnetic resonance (NMR)

¹H and ¹³C solution NMR analyses were performed on a Bruker DPX-400 spectrometer operating at 400 MHz for ¹H and 100 MHz for ¹³C. Samples were prepared in d₆-DMSO, and analysed at 300 K. Chemical shifts are quoted in ppm relative to tetramethylsilane (TMS), and the chemical shifts associated with d₆-DMSO were used as calibration standards. Solid-state ¹H–¹³C CP/MAS spectra were acquired at room temperature with a Chemagnetics CMX-400 spectrometer operating at 400 MHz for ¹H and 100 MHz for ¹³C, with a MAS probehead using zirconia rotors 4 mm in diameter and a spinning speed of 8 kHz. Chemical shifts are quoted in ppm relative to TMS, with hexamethylbenzene (HMB) used as a calibration standard.

Other analytical techniques

Mass spectrometry analyses were performed using a Kratos MS890 spectrometer with samples vaporised directly from the solid state by electron impact. Thermogravimetric analyses were performed using a Polymer Laboratories TGA 1500 apparatus. Samples were heated from room temperature to 200 °C at a heating rate of 10 °C min⁻¹ in a flow of N₂ gas (ca. 25 ml min⁻¹). Melting points were determined using an optical microscope fitted with a hot-stage attachment. Samples were heated at a rate of ca. 5 °C min⁻¹. Elemental analyses were performed using a CE-440 Exeter Analytical elemental analyser.

Acknowledgements

We are grateful to the EPSRC and Avecia Ltd. for funding via a CASE studentship to A. D. B., and to the EPSRC for financial assistance with purchase of the CCD diffractometer. We thank Paul Skelton and Duncan Howe (University of Cambridge) for assistance with the mass spectrometry and solution NMR spectroscopy, respectively. We also acknowledge Dr Robert Docherty and Dr Neil Feeder (Pfizer Global R&D), and Dr John Lawson and Dr Julian Cherryman (Avecia Ltd.) for helpful discussions.

References

- 1 A. Gavezzotti and G. Filippini, *J. Am. Chem. Soc.*, 1995, **117**, 12299.
- 2 W. Jones, in *Organic Molecular Solids: Properties and Applications*, ed. W. Jones, CRC Press, New York, 1997, pp. 149–199.
- 3 Y. Chikaraishi, A. Sano, T. Tsujijama, M. Otsuka and Y. Matsuda, *Chem. Pharm. Bull.*, 1994, **42**, 1123.
- 4 W. C. McCrone, 'Polymorphism', in *Physics and Chemistry of the Organic Solid State*, ed. D. Fox, M. M. Labes and A. Weissberger, Wiley Interscience, New York, 1965, pp. 725–767.
- 5 K. R. Morris, 'Structural aspects of hydrates and solvates', in *Polymorphism in Pharmaceutical Solids*, ed. H. G. Brittain, Dekker, New York, 1999, pp. 125–181.
- 6 W. Jones, C. R. Theocharis, J. M. Thomas and G. R. Desiraju, *J. Chem. Soc., Chem. Commun.*, 1983, 1443.
- 7 A. I. Kitaigorodski, *Mixed Crystals*, Springer, Berlin, 1984.
- 8 J. F. Malone, S. J. Andrews, J. F. Bullock and R. Docherty, *Dyes Pigm.*, 1996, **30**, 183.

- 9 A. D. Bond and W. Jones, *J. Phys. Org. Chem.*, 2000, **13**, 395.
- 10 J. Hartung, R. Kneuer, M. Schwarz, I. Svoboda and H. Feuß, *Eur. J. Org. Chem.*, 1999, 97.
- 11 A. D. Bond and W. Jones, *Acta Crystallogr., Sect. C*, 1999, **55**, 1536.
- 12 B. L. Barnett, H. C. Kretschmar and F. A. Hartman, *Inorg. Chem.*, 1977, **16**, 1834.
- 13 A. D. Bond and W. Jones, *Liq. Cryst. Mol. Cryst.*, 2001, **356**, 305.
- 14 A. Albert, *Selective Toxicity: The Physicochemical Basis of Therapy*, Chapman and Hall, London, 1973.
- 15 A. D. Bond, N. Feeder, S. J. Teat and W. Jones, *Tetrahedron*, 2000, **56**, 6617.
- 16 A. D. Bond and W. Jones, *Acta Crystallogr., Sect. E*, 2001, **57**, m140.
- 17 A. D. Bond and W. Jones, *J. Chem. Soc., Dalton Trans.*, 2001, **20**, 3045.
- 18 A. D. Bond and W. Jones, *Transition Met. Chem.*, 2001, in press.
- 19 G. M. Sheldrick, SHELX-97 Manual, University of Göttingen, Germany, Section 5.2, 1997.
- 20 Cerius², Version 4.0, Molecular Simulations, Inc., San Diego, CA, 1999.
- 21 S. L. Mayo, B. D. Olafson and W. A. Goddard III, *J. Phys. Chem.*, 1990, **94**, 8897.
- 22 P. P. Ewald, *Ann. Phys. (Leipzig)*, 1921, **64**, 253.
- 23 J. J. P. Stewart, *J. Comput.-Aided Mol. Des.*, 1990, **4**, 1.
- 24 M. J. S. Dewar, E. G. Zoebisch, E. F. Healy and J. J. P. Stewart, *J. Am. Chem. Soc.*, 1985, **107**, 3902.
- 25 R. J. Gdanitz, 'Ab initio prediction of possible molecular crystal structures', in *Theoretical Aspects and Computer Modeling of the Molecular Solid State*, ed. A. Gavezzotti, John Wiley and Sons, Chichester, 1997, pp. 185–201.
- 26 Z. Otwinowski and W. Minor, *Macromolecular Crystallography*, in *Methods in Enzymology*, ed. C. W. Carter and R. M. Sweet, Academic Press, London, 1997, Vol. 276, Part A, pp. 307–326.
- 27 R. H. Blessing, *Acta Crystallogr., Sect. A*, 1995, **51**, 33.
- 28 A. Altomare, G. Cascarano, C. Giacovazzo and A. Guagliardi, *J. Appl. Crystallogr.*, 1993, **26**, 343.
- 29 G. M. Sheldrick, SHELXL-97, Program for Crystal Structure Refinement, University of Göttingen, Germany, 1997.